Impact of 3D temperature probe localization variability on MR thermometry validation for RF hyperthermia

Matthew Tarasek[1], Lorne Hofstetter[1], Ruben Pellicer[2], Jurriaan Bakker[2], Wouter Numan[2], Gyula Kotek[2], Eric Fiveland[1], Gavin Houston[3], Gerard van Rhoon[2], Maarten Paulides[2], and Desmond Yeo[1]

[1]*MRI, GE Global Research, Niskayuna, NY, United States,* [2]*Erasmus Medical Center, Rotterdam, Netherlands,* [3]*GE Healthcare, Rotterdam, Netherlands*

Purpose: RF hyperthermia (HT) used in conjunction with other therapy modalities such as radio- or chemo-therapy may increase the efficacy of cancer treatment [1,2]. RF HT typically involves invasive placement of temperature probe catheters for thermometry. In the head and neck region, complex anatomy requires nonlinear catheter trajectories to reach tumours safely [3]. The prevalence of thermo-sensitive tissue in this area necessitates assurance that there is no stray heating outside targeted areas, yet the spatial temperature resolution is limited by the small number of catheters (~4) that can be safely inserted. MR thermometry (MRT) has proven to be an effective and non-invasive method to monitor temperature *in vivo* [4]. MRT can be used to enhance the temperature information available in head and neck treatments by increasing the spatial resolution and accuracy of the temperature information over much larger regions of interest. However, validation of MRT in a head and neck clinical setup requires accurate co-registration of the inserted temperature probes to MRT data. Here, we explore the use of MR imaging techniques and 3D spline fitting for probe localization. In addition, we investigate how uncertainty in the localization affects the registration of probe and MRT readings. **Methods:** Phantoms were made with muscle-simulating "superstuff" (TX-151) interior (cylinder dia=100mm) and oil exterior (outer layer, with dia=135mm) as depicted in Fig. 1a. Catheters were inserted through the muscle-oil phantoms (Fig. 1b) and imaged with a 3D FSPGR sequence (TE = 3.3ms, TR = 6.9, Flip 8°, FOV 33cm, Matrix 512x512, NEX 2, axial slice 2mm) as shown in Fig. 1c. MR imaging parameters were optimized for the measured T_1 and T_2* of the muscle-mimicking region. Points along the path of the catheter were manually extracted from MR images (Fig. 1c), acquired on a 1.5T GE MR450w scanner (GEHC, Waukesha, WI), and 3D cubic spline-curve fitting was performed on these points (Fig. 1d). Each fitted curve was parameterized by the length from the tip of the catheter, which facilitated identification of the locations of four equi-spaced temperature sensors distributed along each fibre-optic temperature probe strand (temp.probe) inserted into each catheter. The phantom was heated using an MR-compatible HYPER*collar* [5] RF hyperthermia applicator (Fig. 2a) and an SPGR imaging sequence (TE = 19.7ms, TR = 110ms, Flip 29°, FOV 40cm, Matrix 128x128, axial slice 10mm) was used to generate proton resonance frequency shift (PRFS) MRT maps. $\mathbf{B_0}$ drift was measured and used to correct PRFS MRT maps [6]. All post-processing was performed with Matlab (Mathworks, Natick, MA).

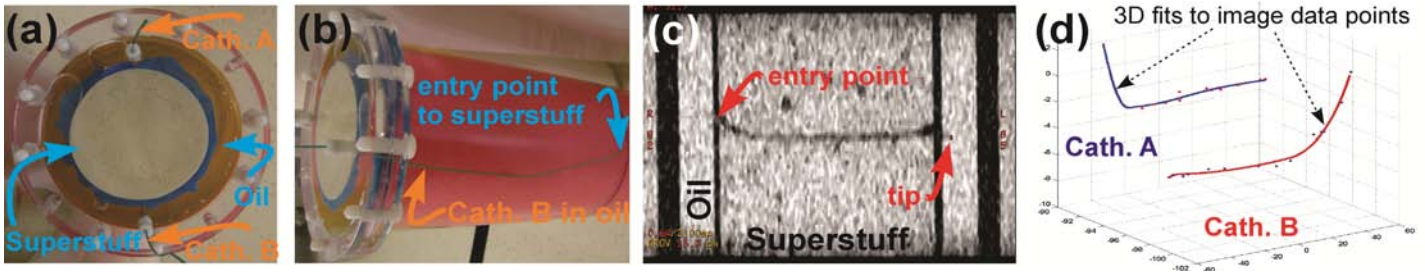

Fig. 1 *(a) Top view of phantom (b) Side view of phantom showing catheter path (c) Coronal FSPGR image showing catheter in phantom (d) Spline fits for catheter/temp.probe localization. The fits are constrained through the localized catheter tip points with <1mm accuracy (in-plane uncertainty in catheter tip was within 1 pixel on a 512 x 512 matrix with 33cm FOV).*

Results: The plots in Fig. 1d show points fit by smoothing cubic spline functions. Fits reconstruct the catheters in MR image coordinate space, and temp.probe location coordinates are extracted from these plots. The data point offset from the spline fit functions (Fig. 1d) show a minimal error from catheter placement. In general, the maximum distance between any segmented position along a catheter and its corresponding spline fit was 0.5mm with an average offset of <0.25mm. Variability in the temp.probe insertion depth within the catheter was large (2mm) compared to the spline fit uncertainty. Fig. 2b shows a PRFS MRT image with the localized position of two temp.probes. Fig. 2c-d shows the maximum temperature variability for MRT data (solid curves) at the temp.probe points from Fig. 2b. Here we assume localization uncertainty in only one direction along the catheter due to the accurate tip location constraint as discussed in Fig. 1d. Analysis was done for all the temp.probe points in this phantom setup. **Conclusions:** For this phantom and heat distribution, temp.probe localization error of 2mm along the catheter length accounts for at most a ±0.5 degree temperature uncertainty in the MRT maps. In some cases a shift in MRT data from the ground-truth temp.probe readings was observed outside the noted measurement uncertainty (eg. Fig. 2c final data point). Other possible sources of MRT/temp.probe measurement mismatch (eg. material-specific α-parameter, B_0 inhomogeneity, B_0 drift, etc.) are under investigation.

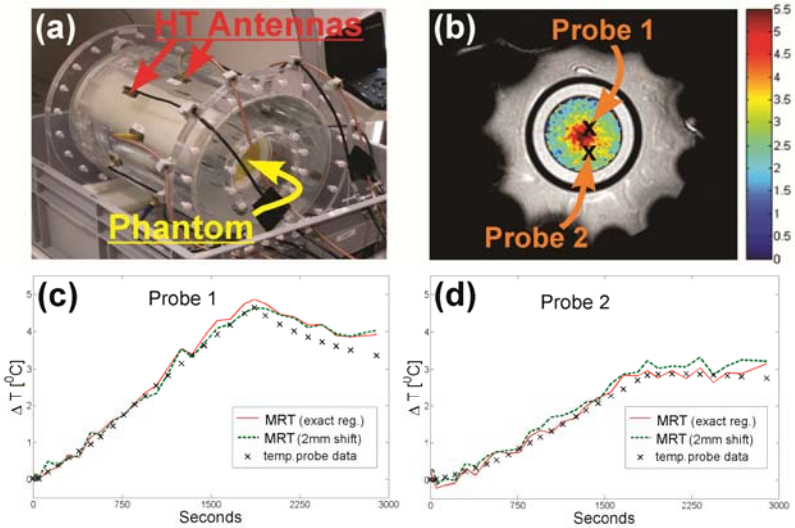

Fig. 2 *(a) MR compatible heating array (b) PRFS MRT map showing probe locations (c)-(d) MRT data (curves) plotted with ground truth temp.probe data for Probes 1 and 2 from (b). Solid curves show the MRT temp. using an exact pixel registration relative to the temp.probe position. The dashed curves plot the MRT temp. using a 2mm shifted pixel registration in one direction along the catheter. See text for justification.*

References: [1] Issels et al. Lanc Onc 2010;11:561-70, [2] Valdangni et al. IJROBP 1993;28:163-69, [3] Paulides et al. Phys Med Biol 2010;55:2465-80, [4] Rieke et al. JMRI 2008;27:376-90, [5] Paulides et al. IJH 2007;68:2, [6] De Poorter et al. MRM 1995;33:74-81